Since January 2020 Elsevier has created a COVID-19 resource centre with free information in English and Mandarin on the novel coronavirus COVID-19. The COVID-19 resource centre is hosted on Elsevier Connect, the company's public news and information website.

Analytica Chimica Acta 1225 (2022) 340267

Contents lists available at ScienceDirect

Analytica Chimica Acta

journal homepage: www.elsevier.com/locate/aca

An extracellular matrix biosensing mimetic for evaluating cathepsin as a host target for COVID-19

Lei Zhou [a,b,*,1], Wenmin Hou [a,1], Ying Wang [c], Xia Lin [c], Jianguo Hu [d], Jinlong Li [e], Chen Liu [c,**], Hongkai Liu [d,***], Hao Li [a,****]

[a] School of Biological Science and Technology, University of Jinan, 336 West Road of Nan, Xinzhuang, 250022, China
[b] Shandong Keyuan Pharmaceutical Co., Ltd, 250022, China
[c] Children's Hospital Affiliated to Shandong University Jinan, Jinan Children's Hospital Jinan, 250002, PR China
[d] Department of Food Science and Nutrition, College of Culture and Tourism, University of Jinan, 13#, Shungeng Road, Jinan, 250000, China
[e] Department of Laboratory Medicine, The Second Hospital of Nanjing, Nanjing University of Chinese Medicine, Nanjing, 210003, PR China

HIGHLIGHTS

- Host protein marker of SARS-CoV-2 can be sensitively detected.
- Picomolar sensitivity can be achieved through photochemical amplfication
- Peptide-based fully synthesizable probe enables cheap and fast detection.
- Direct detection in fractioned clinical tissue samples is possible.

GRAPHICAL ABSTRACT

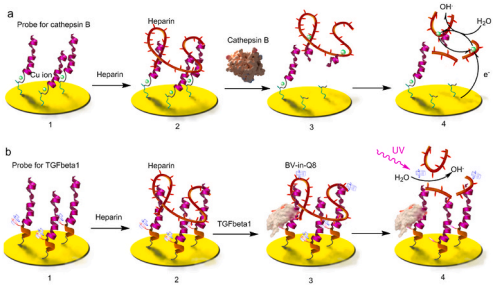

ARTICLE INFO

Keywords:
Cathepsin
Extracellular matrix
COVID-19
Heparin
Cu

ABSTRACT

To combat the new virus currently ravaging the whole world, every possible anti-virus strategy should be explored. As the main strategy of targeting the virus itself is being frustrated by the rapid mutation of the virus, people are seeking an alternative "host targeting" strategy: neutralizing proteins in the human body that cooperate with the virus. The cathepsin family is such a group of promising host targets, the main biological function of which is to digest the extracellular matrix (ECM) to clear a path for virus spreading. To evaluate the potential of cathepsin as a host target, we have constructed a biosensing interface mimicking the ECM, which can detect cathepsin from 3.3 pM to 33 nM with the limit of detection of 1 pM. Based on our quantitative analysis enabled by this biosensing interface, it is clear that patients with background diseases such as chronic inflammation and tumor, tend to have higher cathepsin activity, confirming the potential of cathepsin to serve as a host target for combating COVID-19 virus.

* Corresponding author. School of Biological Science and Technology, University of Jinan, 336 West Road of Nan, Xinzhuang, 250022, China.
** Corresponding author.
*** Corresponding author.
**** Corresponding author.
E-mail addresses: bio_zhoul@ujn.edu.cn (L. Zhou), 61665309@qq.com (C. Liu), cqalhk@163.com (H. Liu), 2603925007@qq.com (H. Li).
[1] These authors have contributed equally to this work and are co-first authors.

https://doi.org/10.1016/j.aca.2022.340267
Received 8 July 2022; Received in revised form 12 August 2022; Accepted 13 August 2022
Available online 16 August 2022

1. Introduction

COVID-19 virus rampages across continents, and the situation is dire [1]: complete extermination of this threat is going to take decades, and effective vaccines are still years away. The therapy we can currently rely upon are mainly small molecule and antibody-based drugs targeting key virus proteins [2], but these proteins mutate so fast that the long-term effectiveness of any such drug cannot be guaranteed [3]. Should this direct targeting strategy fail, the globalized civilization may seem to face the real danger of being overwhelmed by the virus. To increase our chance of winning this anti-virus war, an alternative targeting strategy is urgently needed and can be developed in parallel to the direct targeting strategy. "Host targeting" is such a strategy: the virus relies heavily on proteins of the human body to complete its life cycle, so inhibiting those proteins working with the virus can also check the virus [4]. One promising group of such host target proteins is the cathepsin family of enzymes [5] for regulating the extracellular matrix (ECM). Cells secrete enzymes and other bioactive factors to modify the components of ECM, leading to altered biological properties of the ECM [6] which can in turn influence the spreading of the virus. Central to this cross-talk is the pro-viral spreading interactions of the secreted factors with the ECM components [7]. In the past, information on these interactions is usually inferred from the quantification and activity assay of the various factors fractioned from the sample. The complete image of the interactions can only be pieced together by combing the results of several separated assays. Recently, with the development of biosensing and interface nanotechnology [8,9], it is now possible to construct biosensing interfaces mimicking the ECM. In such a biomimetic sensing system, the secreted bioactive factors could interact with the sensing interface in similar ways as with the ECM, resulting in analogous biophysical and biological changes in the biosensing interface.

An ECM mimicking biosensing interface has been designed here to evaluate the potential of cathepsin B in facilitating virus spreading through digesting the basement membrane [10,11]. The basement membrane consists mainly of proteoiscan which are formed by protein components attached with oligosaccharides such as heparin. Heparin can serve as a temporary reservoir of enzymes and other factors [12]. The secreted enzymes can digest the protein and heparin components of the basement membrane [13], and can also activate the other factors stored in heparin, by enzymatic cleavage [14]. The cytokines and growth factors, etc, thus released, can then complete the cross-talk with the virus-infested cells. A similar process can take place in a biosensing interface as is designed (Scheme 1) here. The interface is formed by designed peptide probes immobilized on the electrode surface. These probes, like the protein components of ECM, contain both the attaching sites of heparin and the motifs that can be recognized and modified by enzymes and other factors. A network mimicking the basement membrane can be constructed from the probes and heparin. The secreted enzymes and bioactive factors from the virus-infested cells can firstly be enriched by heparin that presenting many binding sites of low affinity, as in the case of the native ECM. Then interactions of the secreted factors and the specific sites on the peptide probes can initiate biosensing reactions that can finally digest the heparin network, similar to the digestion of the ECM in the virus spreading process. Through this biomimetic sensing process, the factor secreting activity of virus infested cells can lead to similar biophysical and biological changes as observed in virus spreading.

2. Experimental

Chemicals and biological materials. Peptide probe 1, for cathepsin B (11-Mercaptoundecanoic acid (MUA)K-DAHKI-(ARKKAA-KA)$_3$VLVLVLVL), and probe 2, for TGF beta 1 ((MUA)K–FSHF-(ARK-KAAKA)$_3$VLVLVLVL), were custom-synthesized as lyophilized powder, purity>95%, by Shanghai Science Peptide Co, Ltd. Cathepsin B, TGF beta 1 and anti-TGF beta 1 antibody as its inhibitor, were from R&D system. MUA, 9-mercapto-1-nonanol (MN), benzylviologen (BV) and cucurbit [8]uril (CB [8]) were from Sigma-Aldrich. All the other chemicals were of analytical grade. The solutions of the peptide probe were prepared by dissolving the powder into 10 μM with 10 mM phosphate buffer solution (PBS) (pH 7.4). The label in Scheme 1 b was prepared as follows: Briefly, BV and CB [8] powder of equal molar amounts were dissolved in 10 mM PBS (pH 7.0) to 750 μM followed by moderate vortex-agitating overnight. This solution was freshly prepared each time

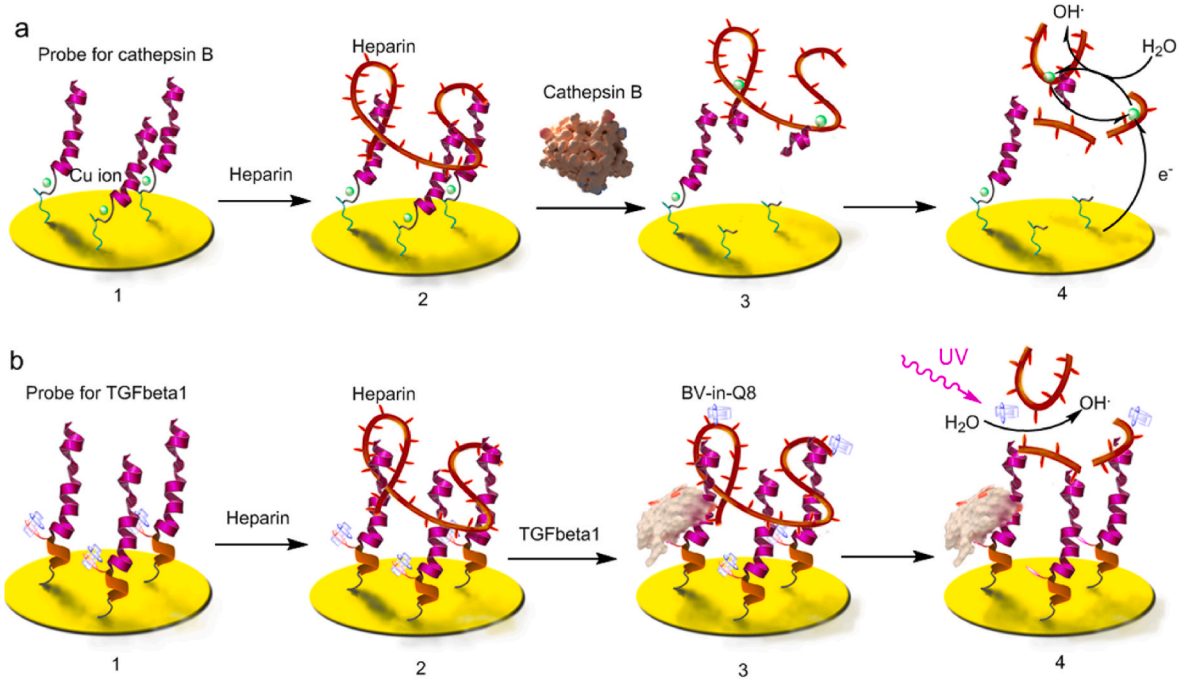

Scheme 1. The proposed method to detect cathepsin and the associated growth factor. (a) The assay for cathepsin. (b) The assay for growth factor. Not drawn to scale.

and was brought to its experimental application immediately after the agitation process. The lyophilized powder of cathepsin was dissolved with 25 mM MES (2-(N-morpholino)ethanesulfonic acid), pH 5.0 to various desired concentrations as the standard samples. The original buffered TGF was dissolved with 10 mM PBS, pH 7.4 to the desired concentrations. All solutions were prepared with double-distilled water, which was purified with a Milli-Q purification system (Branstead, USA) to a specific resistance of 18 MΩ cm. WM793 cell (ATCC) was maintained in Tu2% (80% MCDB153, 20% Leibovitz's L-15, 2% fetal bovine Serum, 5 μg/mL insulin and 1.68 mM $CaCl_2$) medium, and maintained in a humidified atmosphere with 5% CO_2 at 37 °C. For the detection, the cells were plated in 24 well culture plates (Nanjing Protein in Biotechnology Co.) and were incubated with various concentrations of anti-TGF for three days, with the control groups maintained in the same condition in the absence of the antibody. The cell culture medium was then collected for subsequent detection. Cell viability was also assessed by MTT-reducing capacity. For the detection of clinical samples, serum samples were collected from patients (15 for AD and 15 for PD) at The Second Hospital of Nanjing after elected consent by the local ethical committee. 15 serum samples of healthy individuals were also collected as the control.

2.1. Electrode treatment

Transparent Au slides (Aldrich, layer thickness 100 Å) were cut to fit the size of the cuvette used for spectra measurement. These slides were cleaned by sonicating for 20 min in ethanolamine (20 wt %) at around 50 °C, followed by immersion for 10 s in piranha solution (*Caution: piranha solution is dangerous and should be handled with care*). After dried under a mild stream of nitrogen, the slides were immersed in the assembly solution (2.5 μM probe 1 or probe 2 and 5 mM Tris (2-carboxyethyl)phosphine hydrochloride (TCEP) in 10 mM PBS, pH 7.4) at 4 °C for 16 h, TCEP was adopted to prevent disulfide formation between peptide probes. The slides were then immersed in 9-mercaptononanol (MN) solution (1 mM MN in 10 mM PBS, pH 7.4) at room temperature for 3 h. The electrode was then incubated at room temperature for 30 min, with 10 μM $CuCl_2$ in the case of probe 1 modified electrode, or with 750 μM label in the case of probe 2 modified electrode. After gentle rinsing with ddH_2O, incubation with 3.5 μM heparin was conducted for 30 min, followed by gentle rinsing with ddH_2O.

2.2. Detection

Standard samples of cathepsin/TGF or culture media collected from TGF inhibitor incubated cells were incubated with the slide at 37 °C for the proper time. For probe 1 modified electrode, using the slides as the working electrode, the whole mixture was brought under cyclic voltammetric scans with proper scanning parameters, to induce the digestion of the sensing layer. For probe 2 modified electrode, the slide was dipped in 10 mM PBS pH 7.4 and exposed to UV radiation (PLS-LAM500 high-voltage mercury lamp, Perfectlight Co, Ltd.) for 6 min. After gentle rinsing, the slide could be employed for electrochemical measurement.

2.3. Experimental measurements

Isothermal titration calorimetry (ITC) measurements were conducted using a MicroCal ITC200 System (GE healthcare life sciences). The titration was conducted at 25 °C. The titration schedule consisted of 38 consecutive injections of 1 μL with at least a 120 s interval between injections. Heats of dilution, measured by titrating beyond saturation, were subtracted from each data set. All solutions were degassed before titration. The data were analyzed using Origin 7.0 software. Electrochemical measurements were carried out on a CHI660D Potentiostat (CH Instruments) with a conventional three-electrode system: the modified electrode as the working electrode, a saturated calomel electrode (SCE) as the reference electrode, and a platinum wire as the counter electrode. Square wave voltammograms (SWVs) were recorded in 10 mM PBS, pH 7.4, which was deoxygenated by purging with nitrogen gas and maintained under this inert atmosphere during the electrochemical measurements. The experimental parameters for EIS: bias potential, 0.224 V vs. SCE; amplitude, 5 mV; frequency range, 0.1 Hz–10 kHz electrolyte solution: 5 mM $Fe(CN)_6^{3-/4-}$ with 1 M KCl. The data are obtained from at least three times of repetitions of independent experiments, error bars are shown in the figures.

3. Results and discussion

Shown in Scheme 1 is the proposed method to detect secreted cathepsin and the associated growth factor as a means to analyze the potential of cathepsin B in facilitating virus spreading. In scheme 1a is illustrated the assay for the secreted Cathepsin B. Probe 1 is first immobilized on the electrode surface (step a1) by its mercapto group-containing immobilizing motif (green sequence), then Cu (II) ion is complexed (step a1) by the Cu ion binding motif [15] (black sequence), this motif can also serve as the specific substrate of cathepsin [16]the heparin-binding heparin-binding motif [17] (violet sequence), heparin can be assembled on the electrode surface (step a2). So, on the electrode surface is formed a biosensing layer composed of peptide and heparin, presenting the binding and activating sites of secreted factors such as the target enzyme.

The secreted target enzyme can first be enriched by the weak binding sites on the heparin layer, just as in the case in the native basement membrane. Then the activity of the target enzyme can destroy the Cu binding sites (step a3) of the peptide probes, thereby the peptide components of the sensing layer are destroyed. And, similar to the digestion of protein components of the basement membrane can lead to the release of bioactive factors, the Cu ion can be released from the peptide probes, and then bind with the weak binding sites presented in the heparin layer. Using the electrode to provide reducing power, the Cu II ion residing in the heparin layer can be reduced to Cu I, which, due to its instability, automatically become oxidized back to Cu II, simultaneously generating reactive oxygen species [18,19], mainly hydroxyl radical [20]. These radicals can then induce the radical depolymerization of heparin (Step a4).

On the other hand, in the absence of the enzyme cleavage, the peptide probes remain intact. Cu ion complexed in the peptide probes can still generate hydroxyl radical from the solvent H_2O. However, due to its high instability, this reactive species cannot diffuse very far from its site of generation, before reacting with the assembled biomolecules or the solvent [21,22]. Therefore by optimizing the conditions of the electrochemically controllable Cu ion reduction, it may be possible to keep the heparin away from the attacking the reactive oxygen species.

The general layout of the assay for transforming growth factor-beta 1 (TGF beta1), shown in scheme 1b, is similar to that in 1a. The peptide probe also consists of the three motifs for immobilizing (black sequheparin-bindingrin binding (violet sequence), and the motif in between (orange sequence) that is responsible for binding either with the label or with the target protein TGF be1 [23]. This sequhigh-affinityle forms the high affinity binding sites of the TGF, while inside this sequence there are also two tryptophan moieties (for the clearance of presentation, these are represented by one hydroxylphenyl group in Scheme 1) that can bind with the label [24]. This label is benylviologen (BV) complexed by cucurbit [8]uril (Q8) which we have previously employed to recognize other aromatic residual containing peptides in protein biosensing [24]. After formation of the sensing layer (steps b1, b2), the target TGF enriched by heparin can bind with the peptide probes to replace the relatively weak binding labels (step b3), these released labels then become trapped inside the heparin layer. UV radiation can be employed to excite the Q8 caged BV to generate reactive oxygen species [24] (step b4). Following a similar rational as the above Cu catalyzed reaction, this reaction can be tuned to differentially influence the heparin layer in the absence/presence of the target TGF. In

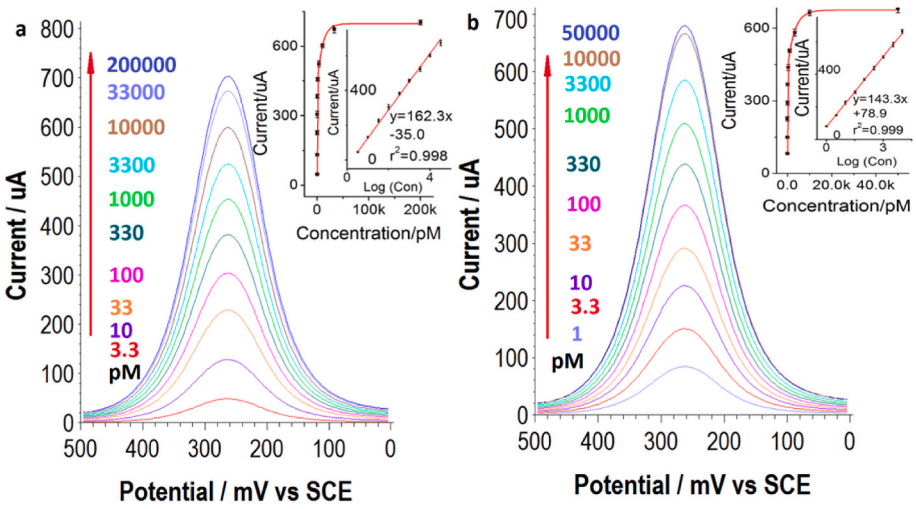

Fig. 1. Square wave voltammograms (SWVs) of $[Fe(CN)_6]^{3-/4-}$ for quantitative analysis of cathepsin (a) and TGF (b), following steps a1∼a5 and b1∼b5 of Scheme 1, respectively. Insets show the peak currents in (a) and (b) as a function of the concentration of their respective targets. Linear regression between the peak currents and the logarithm of target concentration has also been shown. Error bars indicate the standard deviation (n = 3).

both these assays, the target-induced digestion of the sensing layer is probed with an in-solution electroactive reporter $[Fe(CN)_6]^{3-/4-}$ to generate the final signal readout.

The proper functioning of the designed probe has been firstly validated with various experiments. Fig. S1 shows the Cu binding ability of the surface immobilized probe 1 before/after cleavage by the target enzyme. Before enzyme cleavage, relatively strong binding with Cu II ion can be observed, while the enzyme cleavage can completely abolish the binding by destroying the binding sites on the electrode surface. The recognition of the label and the target TGF by probe 2 is studied using isothermal titration calorimetry (ITC), (Figs. S2a and b). Probe 2 can bind strongly to both targets, but its binding with target TGF is stronger. Meanwhile, the interactions between heparin and various species involved in the above design have also been studied (Figs. S2c–f). It can be seen that the Cu ion, the target enzyme, the label, and the target TGF can all have weak interactions with heparin. So the heparin layer of the above design may serve to pre-enrich the target enzyme and TGF, and can also trap the Cu ion or the label released by their respective probe-target interactions.

Electrochemical impedance spectra have also been recorded through the procedure of sensing layer preparation and detection (Fig. S3). For the assay of the target enzyme (Fig. S3a), the bare electrode appears as a straight line on the graph (curve a), indicating nearly no impedance to electron transfer. After surface immobilization of the peptide probes, the impedance increases and manifested as a semicircle of moderate radius (curve b). Subsequent formation of the heparin layer drastically increases the impedance (curve c), due to its strong repulsion with the negatively charged $[Fe(CN)_6]^{3-/4-}$. After interaction with the target enzyme, the impedance shows no evident change (curve d), since the effect of enzyme cleavage and the retaining of the enzyme inside the sensing layer may counteract each other. However, after electrochemically controlled Cu catalyzed depolymerization of heparin, the impedance decreases (curve e), to a level lower than that of the peptide-modified electrode, showing the cleavage of the probes by the target enzyme. For the assay of the target TGF (Fig. S3b), the bare (curve a), peptide modified (curve b), and heparin-coated (curve c) electrodes behave similarly to their respective counterparts above (Fig. S3a curve ãc). The binding of the target TGF also induces an only slight increase of the impedance (curve d), while after UV radiation-induced digestion, the impedance also decreases dramatically (curve e), but does not dropping below the level of the peptide modified electrode.

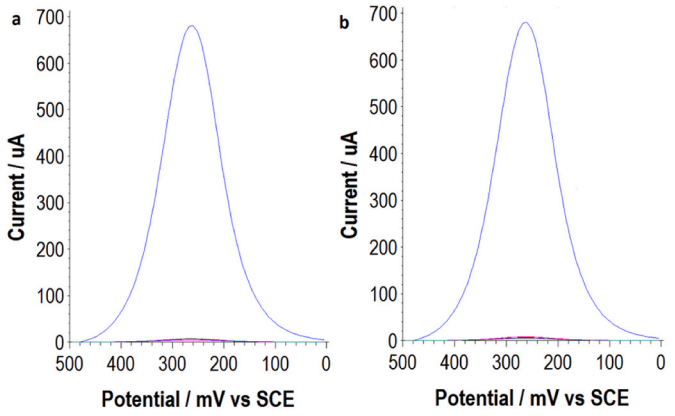

Fig. 2. SWVs of $[Fe(CN)_6]^{3-/4-}$ showing the specificity of the proposed assay in detecting cathepsin (a), TGF (b), and various control species. Control species in (a), blank control (PBS 10 mM, pH 7.4), or 33 nM of TGF, HSA, denatured cathepsin and metalloprotease 9; control species in (b), blank control or 10 nM of cathepsin, HSA, TNF-alpha and denatured TGF.

Experimental conditions of the designed assays are then investigated and optimized. The signal-to-background ratio depends on proper control over the density of the heparin layer and the electrochemical/photochemical digestion, corresponding to the two assays (Scheme 1a, b). The density of the heparin layer is first studied by comparing the signal and background responses of $[Fe(CN)_6]^{3-/4-}$ obtained on sensing layers formed by different concentrations of heparin (Fig. S4, first row). With the increase of heparin surface density, the background is gradually suppressed, but an excessively thick surface layer gradually blocks the signal response, so the largest signal-to-background ratio is obtained before the concentration for heparin surface coating becomes surplus. In the second and the third rows of Fig. S4, the proper control over the electrochemical digestion is investigated by varying parameters such as the range of potential scanning (the second row of Fig. S4) and the duration of the scanning (the third row of Fig. S4). By up-regulating both parameters, the increase of the signal response is more evident than that of the background (Fig. S4b' and S4b''), so the optimal conditions can be obtained before the electrochemical digestion become surplus. The increase of the background under excessive electrochemical conditions may be explained as the Cu ion trapped between the peptide probes began to generate the surplus amount of reactive oxygen species that can start to digest the heparin layer. For the detection of the target TGF, a similar phenomenon can be observed (the fourth row of Fig. S4), and the optimal conditions can be obtained before the parameters of

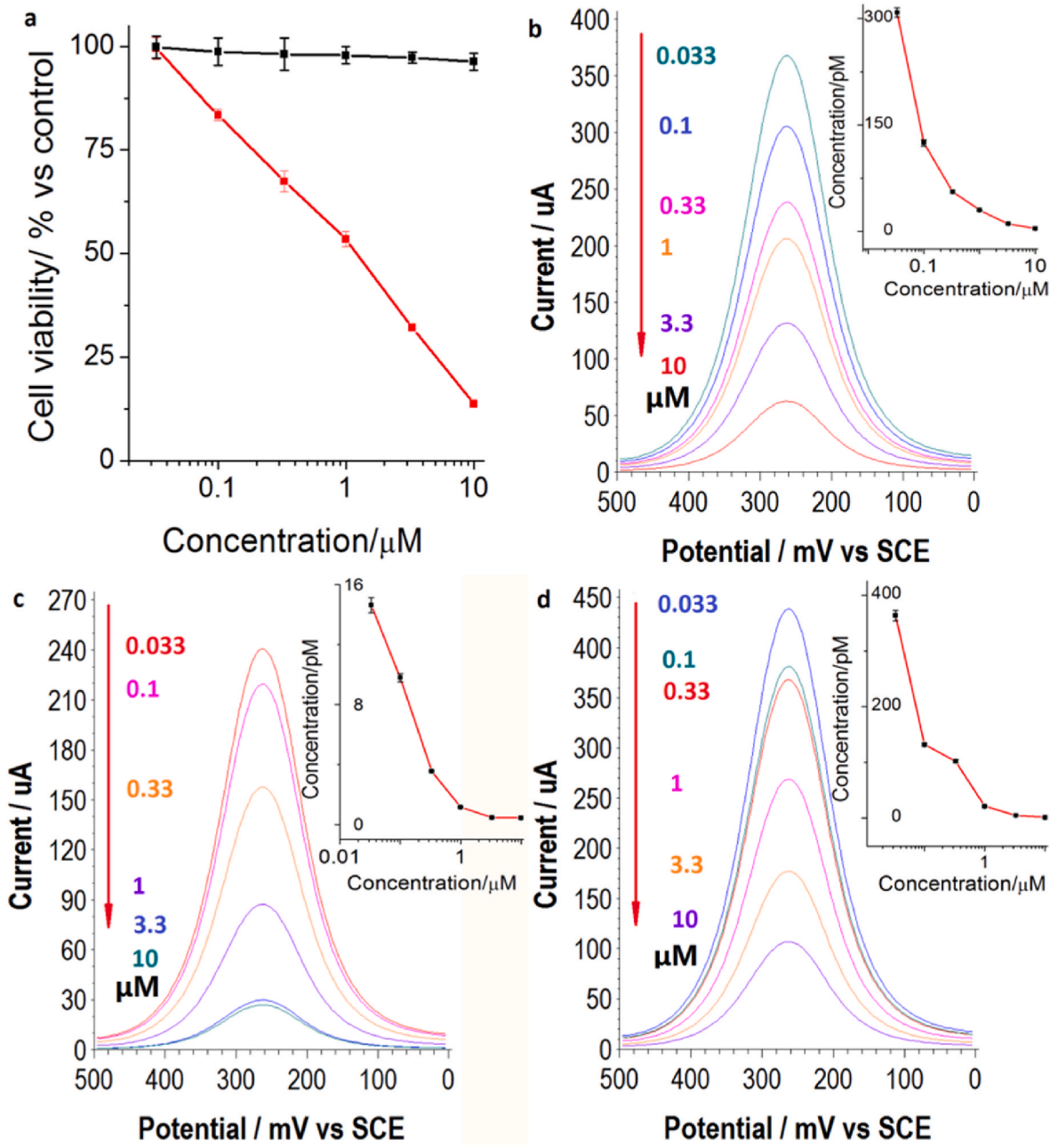

Fig. 3. Detection of the cell secreted cathepsin and TGF, in connection with cell proliferation. (a) MTT assayed cell viability of WM793 (red line) treated with different amounts of TGF inhibitor, as shown on the graph. Controls are from the same culture of the cell but without incubating with the inhibitor (black line). Error bars indicate the standard deviation (n = 3). (b) SWVs are the signal responses in detecting secreted cathepsin in the culture media of the cells treated with the inhibitor, as in (a). Inset shows the detected cathepsin concentration as a function of the amount of inhibitor. The concentrations are obtained by applying the above regression formula to the recorded peak current values. (c) and (d) are similar results obtained in detecting secreted TGF and total secreted TGF, including the latent TGF, respectively. (For interpretation of the references to colour in this figure legend, the reader is referred to the Web version of this article.)

photochemical digestion become surplus.

Under these optimized conditions, the proper incubation time required for the interactions with the target enzyme and TGF is investigated (Fig. S5), and a quantitative signal response can be obtained for the detection of both targets (Fig. 1). For Cathepsin B, a linear range of detection can be established from 3.3 pM to 33 nM (Fig. 1a inset), with the limit of detection (LOD) defined at a signal-to-noise ratio of 3:1 as low as 1 pM, while the linear range for TGF beta 1 is from 1 pM to 10 nM (Fig. 1b inset), LOD: 0.42 pM. For both targets, satisfactory specificity of detection can also be obtained (Fig. 2), with the various control species only yielding negligible signal response similar to the blank control.

COVID-19 patients with background diseases are known to have a higher rate of mortality, while host targets such as cathepsin also have elevated activity in such background diseases as chronic inflammation and tumor. To study this elevated activity in the background disease, the proposed method is then employed in analyzing the factor-secreting activity of human melanoma cell (WM793 cell) in connection with its ability of proliferation. WM793 cells incubated with an inhibitor of the TGF show decreased power of proliferation (Fig. 3a), this is paralleled with decreased secretion of the target enzyme and TGF in an inhibitor dose-dependent manner (Fig. 3b and c and their insets). A sensing layer similar to that shown in Scheme 1b, but with cathepsin B embedded in the heparin layer is also employed to detect the target TGF (Fig. 3d), the result is largely similar to that of Fig. 3b, only that the detected TGF

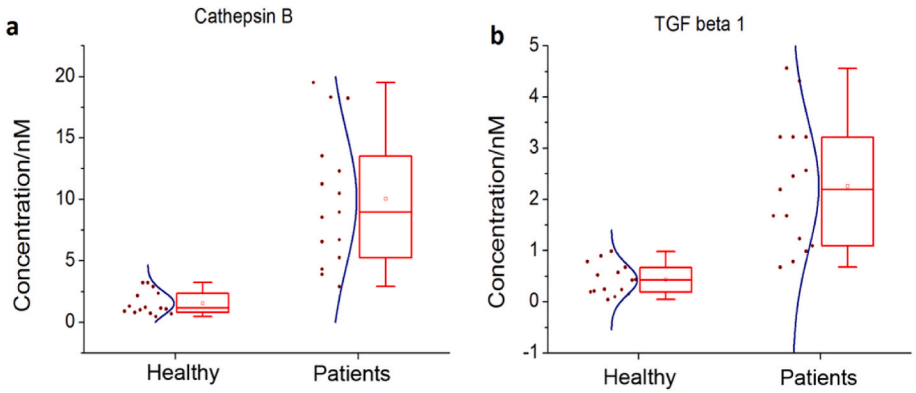

Fig. 4. Box charts showing the distribution of the detected level of cathepsin (a) and TGF (b) in serum samples of patients and healthy volunteers. The raw data is included as a column scatter plot to the left of each box. A curve corresponding to the normal distribution is also displayed on top of the scatter plot.

become more abundant, this may be explained as that the secreted latent TGFs are digested by the heparin-embedded enzyme to mature and to initiate subsequent biosensing steps [25]. So, by a slight modification of the original design, more sophisticated aspects of the factor-secreting activity can be studied using the proposed method. The analytical performance of the proposed method has also been compared with commercially available ELISA assays (Table S1), their performance are comparable.

Elevated cathepsin activity and the associated ECM reformation are frequently observed in many inflammatory conditions that deteriorate the survival rate of COVID patients [26]. Specifically, the virus spreading process always involves both the secretion of enzymes to digest the ECM components and the secretion of various growth factors and cytokines to orchestrate the behavior of the resident cells [27]. Employing the above developed method, clinical serum samples are prepared and the abundance of secreted Cathepsin B and TGF beta 1 is detected (Fig. 4).

4. Conclusion

In this work, we have constructed a bio-mimetic sensing surface to evaluate the potential of cathepsin B as a "host target" for COVID-19. Our quantitative analysis obtained using this biosensing interface shows clearly that those patients with background diseases such as chronic inflammation and tumor tend to have high cathepsin activity, coherent with the fact that COVID-19 mortality is much higher for those with background disease, confirming the potential of cathepsin to serve as a host target for combating COVID-19 virus.

CRediT authorship contribution statement

Lei Zhou: provided the essential idea of the work and have completed the experimentsand. **Wenmin Hou:** provided the essential idea of the work and have completed the experiments. **Ying Wang:** were responsible for acquiring the clinical samples and the experiments done in the clinical laboratories of the hospitals. **Xia Lin:** were responsible for acquiring the clinical samples and the experiments done in the clinical laboratories of the hospitals. **Jianguo Hu:** were responsible for acquiring the clinical samples and the experiments done in th e clinical laboratories of the hospitals. **Jinlong Li:** were responsible for acquiring the clinical samples and the experiments done in the clinical laboratories of the hospitals. **Chen Liu:** Writing – review & editing, Formal analysis, reviewed and analyzed the experimental results and is responsible for writing and proof-reading of the manuscript. **Hongkai Liu:** Writing – review & editing, Formal analysis, reviewed and analyzed the experimental results and is responsible for writing and proof-reading of the manuscript, d. **Hao Li:** Writing – review & editing, Formal analysis, reviewed and analyzed the experimental results and is responsible for writing and proof-reading of the manuscript.

Declaration of competing interest

The authors declare that they have no known competing financial interests or personal relationships that could have appeared to influence the work reported in this paper.

Data availability

No data was used for the research described in the article.

Acknowledgment

This work is supported by the National Natural Science Foundation of China (Grant Nos. 21235003, 81501554), and the Fundamental Research Funds for the Central Universities (Grant No. 021414380001), and Shandong Provincial Natural Science Foundation (Grant No. ZR2021MH131).

Appendix A. Supplementary data

Supplementary data to this article can be found online at https://doi.org/10.1016/j.aca.2022.340267.

References

[1] M. Mukaigawara, I. Hassan, G. Fernandes, L. King, J. Patel, D. Sridhar, Nature Medicine 28 (2022) 893.
[2] M.A. Bakowski, N. Beutler, K.C. Wolff, M.G. Kirkpatrick, E. Chen, T.-T.H. Nguyen, L. Riva, N. Shaabani, M. Parren, J. Ricketts, A.K. Gupta, K. Pan, P. Kuo, M. Fuller, E. Garcia, J.R. Teijaro, L. Yang, D. Sahoo, V. Chi, E. Huang, N. Vargas, A.J. Roberts, S. Das, P. Ghosh, A.K. Woods, S.B. Joseph, M.V. Hull, P.G. Schultz, D.R. Burton, A. K. Chatterjee, C.W. McNamara, T.F. Rogers, Nature Communications 12 (2021) 3309.
[3] W.T. Harvey, A.M. Carabelli, B. Jackson, R.K. Gupta, E.C. Thomson, E.M. Harrison, C. Ludden, R. Reeve, A. Rambaut, S.J. Peacock, D.L. Robertson, C.-G. U. Consortium, Nature Reviews Microbiology 19 (2021) 409.
[4] J. Baggen, E. Vanstreels, S. Jansen, D. Daelemans, Nature Microbiology 6 (2021) 1219.
[5] M.-M. Zhao, W.-L. Yang, F.-Y. Yang, L. Zhang, W.-J. Huang, W. Hou, C.-F. Fan, R.-H. Jin, Y.-M. Feng, Y.-C. Wang, J.-K. Yang, Signal Transduction and Targeted Therapy 6 (2021) 134.
[6] E. Vidak, U. Javoršek, M. Vizovišek, B. Turk, Cells 8 (2019) 264.
[7] K. Prasad, S. Ahamad, D. Gupta, V. Kumar, Heliyon 7 (2021), e08089.
[8] D. Soto, J. Orozco, Analytica Chimica Acta 1205 (2022), 339739.
[9] T. Pinheiro, A.R. Cardoso, C.E.A. Sousa, A.C. Marques, A.P.M. Tavares, A.M. Matos, M.T. Cruz, F.T.C. Moreira, R. Martins, E. Fortunato, M.G.F. Sales, ACS Omega 6 (2021), 29268.
[10] A. Pišlar, A. Mitrović, J. Sabotič, U. Pečar Fonović, M. Perišić Nanut, T. Jakoš, E. Senjor, J. Kos, PLOS Pathogens 16 (2020), e1009013.
[11] C.P. Gomes, D.E. Fernandes, F. Casimiro, G.F. da Mata, M.T. Passos, P. Varela, G. Mastroianni-Kirsztajn, J.B. Pesquero, Frontiers in Cellular and Infection Microbiology 10 (2020).

[12] G. Ghiselli, Medicines (2019) 6.
[13] G.A. Karasneh, D. Kapoor, N. Bellamkonda, C.D. Patil, D. Shukla, Viruses 13 (2021) 1748.
[14] J. Sarker, P. Das, S. Sarker, A.K. Roy, A.Z.M.R. Momen, Scientifica 2021 (2021), 2706789.
[15] A. Trapaidze, C. Hureau, W. Bal, M. Winterhalter, P. Faller, Journal of Biological Inorganic Chemistry 17 (2012) 37.
[16] N. Teich, H. Bodeker, V. Keim, BMC gastroenterology 2 (2002) 16.
[17] B.P. Schick, D. Maslow, A. Moshinski, J.D. San Antonio, Blood 103 (2004) 1356.
[18] H. Li, Y. Huang, Y. Yu, G. Li, Y. Karamanos, Acs Applied Materials & Interfaces 8 (2016) 2833.
[19] H. Li, Y. Huang, Y. Yu, Y. Wang, G. Li, Biosensors & Bioelectronics 80 (2016) 560.
[20] S. Reuter, S.C. Gupta, M.M. Chaturvedi, B.B. Aggarwal, Free Radical Biology and Medicine 49 (2010) 1603.
[21] M. Valko, M. Izakovic, M. Mazur, C.J. Rhodes, J. Telser, Molecular and Cellular Biochemistry 266 (2004) 37.
[22] L.J. Marnett, Carcinogenesis 21 (2000) 361.
[23] G.D. Young, J.E. Murphy-Ullrich, Journal of Biological Chemistry 279 (2004), 47633.
[24] H. Li, H. Xie, Y. Huang, B. Bo, X. Zhu, Y. Shu, G. Li, Chemical Communications 49 (2013) 9848.
[25] K. Tzavlaki, A. Moustakas, Biomolecules 10 (2020) 487.
[26] X. Ding, N. Ye, M. Qiu, H. Guo, J. Li, X. Zhou, M. Yang, J. Xi, Y. Liang, Y. Gong, J. Li, Chemico-Biological Interactions 353 (2022), 109796.
[27] S. Seth, J. Batra, S. Srinivasan, Frontiers in Molecular Biosciences 7 (2020).